Numer. Math. Theor. Meth. Appl. doi: 10.4208/nmtma.2024-0033

The Stabilized Finite Element Method for the Cahn-Hilliard Phase-Field Model of Diblock Copolymers on Evolving Surfaces

Lulu Liu, Xufeng Xiao* and Xinlong Feng

College of Mathematics and System Sciences, Xinjiang University, Urumqi 830046, P.R. China

Received 24 March 2024; Accepted (in revised version) 14 October 2024

Abstract. This work focuses on the efficient numerical simulation of the Cahn-Hilliard phase-field model of diblock copolymers on evolving surfaces. The model integrates Cahn-Hilliard dynamic of diblock copolymers with partial differential equation on evolving surfaces, which has the property of geometric complexity, nonlinearity and mass conservation. In the numerical simulation, the space-time discretization of the proposed model is realized by the evolving surface finite element method. The stabilized semi-implicit approach is included in the framework of the evolving surface finite element method to produce a linear, stable, conserved and high-accurate scheme for long time numerical simulations. The stability analysis of the designed numerical method is established. Through several numerical experiments, the convergence and stability of the numerical method are investigated. In addition, spinodal decomposition is performed to research the mass evolution and dynamics of the Cahn-Hilliard model of diblock copolymers on different evolving surfaces.

AMS subject classifications: 35J05, 65N30, 92E10

Key words: Cahn-Hilliard model of diblock copolymers, evolving surface finite element method, stability analysis, long time numerical simulations.

1. Introduction

A diblock copolymer is a copolymer formed by the alternating arrangement of two different monomers repeatedly. It is widely used in nanotechnology [1,2,7], biomathematics [13,25], film materials [30,34], and other fields due to its many unique properties. The Cahn-Hilliard (CH) phase-field model of diblock copolymers is a mathematical model to describe the related evolution behaviors [3,4,23,35]. It is based on the CH

^{*}Corresponding author. Email addresses: liululumath@sina.com (L. Liu), xiaoxufeng111@sina.com (X. Xiao), fxlmath@xju.edu.cn (X. Feng)

L. Liu, X. Xiao and X. Feng

equation with considering the concentration profiles of two different monomers on the copolymer chain. The idea of modeling is to introduce an order parameter to represent the difference between the concentration of the two categories of monomers. The evolution of the system can be viewed as the minimization of the total free energy functional in CH dynamics. The energy of the system is given by the nonlocal Ohta-Kawasaki functional which containing a nonlocal term that represents the first-order effects of the connectedness of the monomer chains [4, 6]. In [4, 24, 37], the authors have investigated the CH phase-field model of diblock copolymers, including the establishment of mathematical models, the design of reliable and effective numerical methods, and the numerical simulation in two- and three-dimensions.

The modeling of diblock copolymers on evolving domains is more general than that on two- and three-dimensional stationary domains. Therefore, it is interesting to investigate the dynamic behavior of this model on evolving surfaces, which corresponds to simulation studies on non flat and evolving substrates. This study is devoted to present the related mathematical modeling and numerical simulation approach. To explore the performance of the diblock copolymers on evolving surfaces, we construct the model by combining the CH dynamics of diblock copolymers and the partial differential equations on evolving surfaces. On the evolving surface, the developed model has the physical property of mass conservation. However, the velocity can be regarded as a force that is external, so the energy is not strictly dissipated. The property of energy is not studied in this paper, and more related content can be found in [19, 20].

To solve the CH model of diblock copolymers on the evolving surface, the related space-time discretization approaches should be reviewed. The evolving surface finite element method (ESFEM) [9–11, 27], stands as a widely-used space-time discretization technique that relies on a triangular mesh and variational formulation. Meshless methods are a class of methods that avoid mesh generation and have high accuracy. The common meshless approaches include the element-free Galerkin method [26, 31], the radial basis function finite differences (RBF-FD) method [22, 29], the moving least squares method [14,15]. Although they avoid mesh generation, the numerical stability depends strongly on the distribution of surface nodes in the local stencil, and the related theoretical analyses are hard to be given. Taking into account both the operability of programming and the complexity of theoretical investigation, we select ESFEM as the fundamental method for space-time discretization in this study.

Another difficulty in designing the numerical method is avoiding the numerical instability caused by the small interface parameter for long time simulation. There are some mature and efficient numerical methods for settling models in 2D and 3D. Invariant energy quadratization (IEQ) [4,24] and scalar auxiliary variable (SAV) methods [23] are widely used in the design of numerical algorithms. The fundamental idea behind these two approaches is to create a new equation that is of equal value to the original equation by bringing in suitable auxiliary variables and formulating the energy functional into a quadratic form. For the IEQ and SAV schemes, the numerical solution can only guarantee that the modified energy is monotonically nonincreasing, but it cannot obtain stability with respect to the original energy.

The fully implicit or fully explicit discrete methods [21,28] have high requirements on the step size and have no marked superiority in the stable and long-term numerical simulation. The traditional semi-implicit (SI) scheme [5,26] combines the strengths of full implicit and full explicit but still has a little limit on step size. The stabilized semi-implicit (SSI) method [12,18,33,36] is obtained by adding stabilized terms to the SI method, which can effectively settle the instability caused by the rigidity of the model. As previously stated, this paper does not consider the related properties of energy, and this method can well balance the rigidity of the model, which is suitable for dealing with this problem. Therefore, utilizing the ESFEM framework in conjunction with the SSI scheme, we devise an efficient numerical method for evolving surfaces.

The rest of this paper is organized as follows. In Section 2, the CH model of diblock copolymers on evolving surfaces is constructed, and the mass conservation property is proved. In Section 3, the corresponding numerical algorithm is designed for the model. In Section 4, the stability of the numerical method is analyzed. Section 5 presents numerical simulations that aim to demonstrate the validity of the model and the efficacy of the numerical method. Furthermore, the dynamics of the proposed model are investigated by experiments of spinodal decomposition on different evolving surfaces.

2. The CH model of diblock copolymers on evolving surfaces

In this part, the CH model of diblock copolymers on evolving surfaces is introduced. For $\forall t \in [0,T], T>0$, let $\Gamma(t)$ be a smooth closed evolving hypersurface in $\mathcal{N}(t) \subset \mathbb{R}^3$. The velocity field v determines the orientation of the evolution of the surface $\Gamma(t)$, and $\Gamma_0 = \Gamma(0)$ is the initial surface. Introduce the level set function $\eta(\mathbf{x},t) \in C^4(\mathcal{N}(t))$, $\nabla \eta(\mathbf{x},t) \neq 0$, such that $\Gamma(t)$ has the following zero-level set expression:

$$\Gamma(t) = \{ (\mathbf{x}, t) = (x, y, z, t) \in \mathcal{N}(t) \mid \eta(\mathbf{x}, t) = 0 \}$$

and

$$\begin{cases} \eta(\mathbf{x}, t) > 0, & \mathbf{x} \in \mathcal{N}^+(t), \\ \eta(\mathbf{x}, t) < 0, & \mathbf{x} \in \mathcal{N}^-(t), \end{cases}$$

where $\mathcal{N}^+(t)$ and $\mathcal{N}^-(t)$ denote that the surface $\Gamma(t)$ divides $\mathcal{N}(t)$ into inner and outer parts such that $\mathcal{N}^+(t) \cap \mathcal{N}^-(t) = \emptyset$ and $\mathcal{N}^+(t) \cup \Gamma(t) \cup \mathcal{N}^-(t) = \mathcal{N}(t)$ are satisfied. The unit normal vector at $\forall (\mathbf{x},t) \in \Gamma(t)$ is $\mathbf{n}(\mathbf{x},t) = \nabla \eta(\mathbf{x},t)/|\nabla \eta(\mathbf{x},t)|$.

To facilitate the description of the following notation, the space-time region \mathcal{R}_T is defined as

$$\mathcal{R}_T = \bigcup_{t \in [0,T]} \Gamma(t) \times \{t\}.$$

Take the function $u: \mathcal{R}_T \to \mathbb{R}$ and define the material derivative

$$\partial^{\bullet} u = \frac{\partial u}{\partial t} + u \nabla \cdot v. \tag{2.1}$$

For any function u on the surface $\Gamma(t)$, define its tangential gradient and tangential divergence as $\nabla_{\Gamma(t)}u = \nabla u - \nabla u \cdot \boldsymbol{n}\boldsymbol{n}^{\top}$ and $\nabla_{\Gamma(t)}u = \operatorname{trace}(\nabla_{\Gamma(t)}u)$. Laplace-Beltrami operator of u is defined as $\Delta_{\Gamma(t)}u = \nabla_{\Gamma(t)} \cdot \nabla_{\Gamma(t)}u$.

In [8], the differentiation of time dependent surface integrals can be achieved by the use of the transport formulae, which have been demonstrated.

Lemma 2.1. Consider an evolving surface, denoted as $\Gamma(t)$, which possesses a velocity field given by $v(\mathbf{x},t)$, for smooth functions $u(\mathbf{x},t)$ and $g(\mathbf{x},t)$, there are

$$\frac{\mathrm{d}}{\mathrm{d}t} \int_{\Gamma(t)} u \mathrm{d}\mathbf{x} = \int_{\Gamma(t)} \partial^{\bullet} u + u \nabla_{\Gamma(t)} \cdot v \, \mathrm{d}\mathbf{x}, \tag{2.2}$$

$$\frac{\mathrm{d}}{\mathrm{d}t} \int_{\Gamma(t)} ug \mathrm{d}\mathbf{x} = \int_{\Gamma(t)} \partial^{\bullet} ug + u\partial^{\bullet} g + ug \nabla_{\Gamma(t)} \cdot v \, \mathrm{d}\mathbf{x}. \tag{2.3}$$

The CH model of diblock copolymers is constructed by the phase field method. Phase field variable $\phi \in L^2(\Gamma)$ is introduced to represent the concentration difference of two monomers. The evolution of the system is governed by a coarse-grained free energy functional, expressed as follows:

$$E(\phi) = \int_{\Gamma(t)} \left(\frac{\epsilon}{2} |\nabla \phi|^2 + \frac{1}{\epsilon} F(\phi) \right) d\mathbf{x}$$
$$+ \frac{\alpha \epsilon}{2} \int_{\Gamma(t)} \int_{\Gamma(t)} G(\mathbf{x} - \mathbf{y}) (\phi(\mathbf{x}) - \bar{\phi}) (\phi(\mathbf{y}) - \bar{\phi}) d\mathbf{x} d\mathbf{y}, \tag{2.4}$$

where $F(\phi)=(\phi^2-1)^2/4$ is the bulk Ginzburg-Landau double well potential,

$$ar{\phi} = rac{1}{|\Gamma(t)|} \int_{\Gamma(t)} \phi \, \mathrm{d}\mathbf{x}, \quad G(m{x} - m{y}) = -\delta(m{x} - m{y})$$

is Green's function, α is a positive parameter and ϵ is interface width. By using the Cahn-Hilliard dynamics for ϕ , the CH model of diblock copolymers on evolving surfaces is governed by equations

$$\begin{cases} \partial^{\bullet} \phi + \phi \nabla_{\Gamma(t)} \cdot v = M \Delta_{\Gamma(t)} \psi, \\ \psi = \frac{\delta E(\phi)}{\delta \phi}, \end{cases}$$
 (2.5)

where M represents mobility. The final model system is governed by the following equations:

$$\begin{cases}
\partial^{\bullet} \phi + \phi \nabla_{\Gamma(t)} \cdot v = M \Delta_{\Gamma(t)} \left(\psi + (-\Delta_{\Gamma(t)})^{-1} \alpha \epsilon (\phi - \bar{\phi}) \right), & \mathbf{x} \in \Gamma(t), \ t \in (0, T], \\
\psi = -\epsilon \Delta_{\Gamma(t)} \phi + \frac{f(\phi)}{\epsilon}, & \mathbf{x} \in \Gamma(t), \ t \in (0, T], \\
\phi = \phi_{0}, & \mathbf{x} \in \Gamma(t), \ t = 0,
\end{cases}$$
(2.6)

where $f(\phi) = F(\phi)' = \phi^3 - \phi$. The velocity can be perceived as an external force, thus the energy is not solely dissipated. Hence, the property of energy is not the focus of this paper. The model (2.6) satisfies the mass conservation property. The following theorem gives the proof.

Theorem 2.1. The model presented in (2.6) fulfills the mass conservation property, namely,

$$\frac{\mathrm{d}}{\mathrm{d}t} \int_{\Gamma(t)} \phi \, \mathrm{d}\mathbf{x} = 0. \tag{2.7}$$

Proof. Using Lemma 2.1 and (2.6), we obtain

$$\frac{\mathrm{d}}{\mathrm{d}t} \int_{\Gamma(t)} \phi \varphi \, \mathrm{d}\mathbf{x} + \int_{\Gamma(t)} \nabla_{\Gamma(t)} \psi \nabla_{\Gamma(t)} \varphi \, \mathrm{d}\mathbf{x}$$

$$= -\alpha \epsilon \left(\int_{\Gamma(t)} (\phi - \bar{\phi}) \varphi \, \mathrm{d}\mathbf{x} \right) + \int_{\Gamma(t)} \phi \partial^{\bullet} \varphi \, \mathrm{d}\mathbf{x}. \tag{2.8}$$

Let $\varphi = 1$, and Eq. (2.8) can be rewritten as

$$\frac{\mathrm{d}}{\mathrm{d}t} \int_{\Gamma(t)} \phi \, \mathrm{d}\mathbf{x} = -\alpha \epsilon \left(\int_{\Gamma(t)} \phi \, \mathrm{d}\mathbf{x} - \frac{1}{|\Gamma(t)|} \int_{\Gamma(t)} \phi \, \mathrm{d}\mathbf{x} \int_{\Gamma(t)} \, \mathrm{d}\mathbf{x} \right) = 0.$$
 (2.9)

The mass conservation property is proved.

3. Numerical method

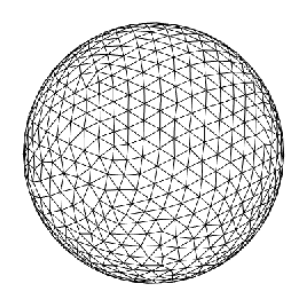
In this section, the numerical methods for solving the CH model of diblock copolymers is presented. On the basis of ESFEM, we combine the SSI method to construct the numerical schemes.

3.1. Evolving surface finite element method (ESFEM)

Choosing the test functions η , ξ in $H^1(\Gamma(t))$, and using Lemma 2.1, the weak form of (2.6) is denoted by

Choosing the test functions
$$\eta$$
, ξ in $H^{1}(\Gamma(t))$, and using Lemma 2.1, the weak form (2.6) is denoted by
$$\begin{cases} \frac{\mathrm{d}}{\mathrm{d}t} \int_{\Gamma(t)} \phi \eta \, \mathrm{d}\mathbf{x} + M \int_{\Gamma(t)} \nabla_{\Gamma(t)} \psi \nabla_{\Gamma(t)} \eta \, \mathrm{d}\mathbf{x} + M \alpha \epsilon \left(\int_{\Gamma(t)} (\phi - \bar{\phi}) \eta \, \mathrm{d}\mathbf{x} \right) \\ = \int_{\Gamma(t)} \phi \partial^{\bullet} \eta \, \mathrm{d}\mathbf{x}, \\ \int_{\Gamma(t)} \psi \xi \, \mathrm{d}\mathbf{x} = \epsilon \int_{\Gamma(t)} \nabla_{\Gamma(t)} \phi \nabla_{\Gamma(t)} \xi \, \mathrm{d}\mathbf{x} + \frac{1}{\epsilon} \int_{\Gamma(t)} f \xi \, \mathrm{d}\mathbf{x}. \end{cases}$$
(3.1)

It is difficult to directly divide the mesh, define the basis function, and perform integration on the original surface Γ . Therefore, the first step of the ESFEM is to perform



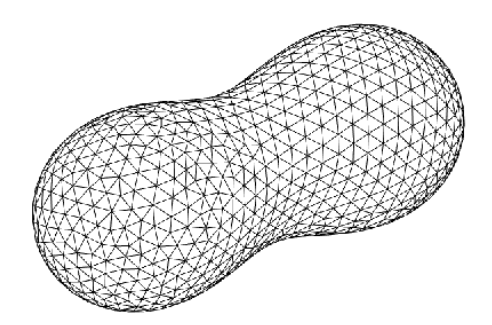


Figure 1: Triangulated mesh discretization of surfaces.

the surface approximation, that is, to use the discrete surface spliced by the quasiuniform piecewise triangular mesh to approximately replace Γ as the computational area. The discretized surface, denoted Γ_h , is composed of non-overlapping and quasiuniform triangles $\mathbf{e}_{h,k}(t)$, as shown in Fig. 1. The discrete surface generation technique used in this paper is a matching algorithm for level set surfaces, which can be referred to [16] for details.

Denote the set of triangles as $\{\mathbf{e}_{h,k}(t)\}_{k=1}^{N_e}$, then the discrete mesh can be represented as

$$\Gamma_h(t) = \bigcup_{k=1}^{N_e} \mathbf{e}_{h,k}(t),$$

where N_e is the number of triangles. The mesh size parameter of the discretized surface Γ_h is h, $h:=\max_{k=1}^{N_e}h_k$, where h_k is the longest edge of $\mathbf{e}_{h,k}(t)$. When t=0, Γ_h^0 is a polyhedral approximation of the initial surface Γ^0 and restricts the nodes $\{\mathbf{X}_j^0\}_{j=1}^{N_p}$ of Γ_h^0 to lie on Γ^0 . We evolve the node $\{\mathbf{X}_j(t)\}_{j=1}^{N_p}$ by the surface velocity

$$\frac{\mathrm{d}\mathbf{X}_j}{\mathrm{d}t}(t) = v(\mathbf{X}_j(t), t), \quad j = 1, \dots, N_p,$$
(3.2)

where N_p is the number of nodes. Let \widehat{N} be a positive integer and T be the total time, the time step $\Delta t := T/\widehat{N}$ and $t^n = n\Delta t$. The finite element space is defined as

$$S_h(t) = \left\{ \phi_h(\mathbf{X}, t) \in C^0(\Gamma_h(t)) \mid \phi_h(\mathbf{X}, t) \text{ is linear polynomial on } \mathbf{e}_h(t), \right.$$

$$\forall \mathbf{e}_{h,k}(t) \in \left\{ \mathbf{e}_{h,k}(t) \right\}_{k=1}^{N_e} \right\}$$

$$= \operatorname{Span} \left\{ \chi_j(\mathbf{X}, t) \mid j = 1, 2, \dots, N_p \right\} \subset H^1(\Gamma_h(t)). \tag{3.3}$$

The node basis functions in the space S_h are defined by

$$\chi_j(\mathbf{X}_k, t) = \begin{cases} 1, & j = k, \\ 0, & j \neq k, \end{cases} \quad j, k = 1, 2, \dots, N_p.$$
 (3.4)

Let $S_h^n = S_h(t^n)$, $Z_h^n = Z_h(\mathbf{x}, t^n)$, $Y_h^n = Y_h(\mathbf{x}, t^n) \in S_h^n$. We define the following bilinear forms:

$$m_h(Z_h^n, Y_h^n) = \int_{\Gamma_h(t)} Z_h^n Y_h^n d\mathbf{x},$$

$$a_h(Z_h^n, Y_h^n) = \int_{\Gamma_h(t)} \nabla_{\Gamma_h(t)} Z_h^n \cdot \nabla_{\Gamma_h(t)} Y_h^n d\mathbf{x}.$$
(3.5)

Next, the discrete solution of the finite element can be expressed as

$$\phi_h^n = \sum_{j=1}^{N_p} \phi_j^n \chi_j^n \in S_h^n, \quad \psi_h^n = \sum_{j=1}^{N_p} w_j^n \chi_j^n \in S_h^n,$$
 (3.6)

where ϕ_j^n and ψ_j^n are nodal values at t^n . An arbitrary point $\mathbf{x} = \mathbf{X}(t) \in \Gamma_h(t)$, material velocity $v_h(\mathbf{x},t)$ is given by

$$\frac{\mathrm{d}}{\mathrm{d}t}\mathbf{X}(t) = v_h\left(\mathbf{x},t\right), \quad v_h\left(\mathbf{X}(t),t\right) := \sum_{j=1}^{N_p} \frac{\mathrm{d}}{\mathrm{d}t}\mathbf{X}_j(t)\chi_j\left(\mathbf{x},t\right). \tag{3.7}$$

We define the space-discrete material derivative on each element of $\Gamma_h(t)$ as

$$\partial_h^{\bullet} Y_h(\mathbf{x}, t)|_{\mathbf{e}_h(t)} = \frac{\partial}{\partial t} Y_h(\mathbf{x}, t) + v_h(\mathbf{x}, t) \cdot \partial Y_h(\mathbf{x}, t). \tag{3.8}$$

The basis functions satisfy the transport property that [9, 10]

$$\partial_b^{\bullet} \chi_j(\mathbf{x}, t) = 0, \quad j = 1, \dots, N.$$
 (3.9)

With this property, there will be no velocity or curvature term in the evolving surface finite element scheme. In addition, for $Y_h^n \in S_h^n$, $Y_h^{n+1} \in S_h^{n+1}$, we define

$$\partial_h^{\bullet} Y_h^n = \sum_{j=1}^N \frac{1}{\Delta t} \left(Y_j^{n+1} - Y_j^n \right) \chi_j^n \in S_h^n, \tag{3.10}$$

which will be used for theoretical analysis.

3.2. Stabilized semi-implicit (SSI) scheme

The purpose of introducing the SSI method is to avoid the numerical instability caused by the small interface width and nonlinearity. The substance of the SSI method is to add the corresponding stabilized terms based on the original scheme. This method can significantly improve the stability, which is beneficial to long time numerical simulations.

The first-order scheme of the SSI method for (3.1) is shown in

$$\begin{cases}
\frac{1}{\Delta t} \left(m_h(\phi_h^{n+1}, \eta_h^{n+1}) - m_h(\phi_h^n, \eta_h^n) \right) + M a_h(\psi_h^{n+1}, \eta_h^{n+1}) \\
+ M \alpha \epsilon \left(m_h(\phi_h^n, \eta_h^n) - m_h(\bar{\phi}_h^n, \eta_h^n) \right) = m_h(\phi_h^n, \partial_h^{\bullet} \eta_h^n), \\
m_h(\psi_h^{n+1}, \xi_h^{n+1}) = \epsilon a_h(\phi_h^{n+1}, \xi_h^{n+1}) + \frac{1}{\epsilon} m_h(f(\phi_h^n), \xi_h^n) \\
+ \frac{\beta}{\epsilon} \left(m_h(\phi_h^{n+1}, \xi_h^{n+1}) - m_h(\phi_h^n, \xi_h^n) \right),
\end{cases} (3.11)$$

where β is the coefficient of the stabilized terms. And the second-order scheme of the SSI method is as follows:

$$\begin{cases}
\frac{1}{2\Delta t} \left(3m_h(\phi_h^{n+1}, \eta_h^{n+1}) - 4m_h(\phi_h^n, \eta_h^n) + m_h(\phi_h^{n-1}, \eta_h^{n-1}) \right) \\
+ Ma_h(\psi_h^{n+1}, \eta_h^{n+1}) + 2M\alpha\epsilon \left(m_h(\phi_h^n, \eta_h^n) - m_h(\bar{\phi}_h^n, \eta_h^n) \right) \\
- M\alpha\epsilon \left(m_h(\phi_h^{n-1}, \eta_h^{n-1}) - m_h(\bar{\phi}_h^{n-1}, \eta_h^{n-1}) \right) \\
= 2m_h(\phi_h^n, \partial_h^{\bullet} \eta_h^n) - m_h(\phi_h^{n-1}, \partial_h^{\bullet} \eta_h^{n-1}), \\
m_h(\psi_h^{n+1}, \xi_h^{n+1}) = \epsilon a_h(\phi_h^{n+1}, \xi_h^{n+1}) \\
+ \frac{1}{\epsilon} \left(2m_h(f(\phi_h^n), \xi_h^n) - m_h(f(\phi_h^{n-1}), \xi_h^{n-1}) \right) \\
+ \frac{\beta\Delta t}{\epsilon} \left(m_h(\phi_h^{n+1}, \xi_h^{n+1}) - m_h(\phi_h^n, \xi_h^n) \right).
\end{cases} \tag{3.12}$$

Theorem 3.1. The first-order (3.11) and second-order (3.12) of the numerical scheme fulfill the mass conservation property, namely,

$$m_h(\phi_h^i, 1) = m_h(\phi_h^0, 1), \quad i = 1, 2, \dots, n.$$
 (3.13)

$$m_{h}(\phi_{h}, 1) = m_{h}(\phi_{h}, 1), \quad t = 1, 2, ..., n.$$
(3.13)
$$Proof. \text{ Let } \eta_{h}^{n+1} = \eta_{h}^{n} = \eta_{h}^{n-1} = 1. \text{ For the first-order scheme, we get}$$

$$\frac{1}{\Delta t} \left(m_{h}(\phi_{h}^{n+1}, 1) - m_{h}(\phi_{h}^{n}, 1) \right) + M\alpha \epsilon \left(m_{h}(\phi_{h}^{n}, 1) - m_{h}(\bar{\phi}_{h}^{n}, 1) \right) = 0,$$
(3.14)

which indicates that $m_h(\phi_h^n, 1) = m_h(\phi_h^0, 1)$, that is, the discrete first-order scheme (3.11) follows from the mass conservation property.

For the second-order scheme, we obtain

$$3m_h(\phi_h^{n+1}, 1) - 4m_h(\phi_h^n, 1) + m_h(\phi_h^{n-1}, 1) = 0.$$
(3.15)

During the algorithm implementation, we figure out ϕ_h^1 using the first-order scheme by a small time step, then

$$m_h(\phi_h^1, 1) = m_h(\phi_h^0, 1).$$
 (3.16)

When n = 1, it can be obtained

$$m_h(\phi_h^2, 1) = m_h(\phi_h^0, 1).$$
 (3.17)

Then we can deduce that

$$m_h(\phi_h^n, 1) = m_h(\phi_h^0, 1), \quad n = 1, 2, \dots, N,$$
 (3.18)

which indicates that the second-order scheme (3.12) satisfies the mass conservation property.

For numerical schemes (3.11) and (3.12), we will next write their matrix forms. Let

$$\mathcal{M}(t) = \left(\mathcal{M}(t)^{jk}\right)_{N_p \times N_p}, \quad \mathcal{S}(t) = \left(\mathcal{S}(t)^{jk}\right)_{N_p \times N_p},$$

$$\mathcal{I}(t) = \left(\mathcal{I}(t)^j\right)_{N_p \times 1}, \qquad \mathcal{F}_i(t) = \left(\mathcal{F}_i(t)^j\right)_{N_p \times 1}$$
(3.19)

be the matrices with the entries

$$\mathcal{M}(t)^{jk} = \int_{\Gamma_h(t)} \chi_j(\mathbf{x}, t) \chi_k(\mathbf{x}, t) d\mathbf{x},$$

$$\mathcal{S}(t)^{jk} = \int_{\Gamma_h(t)} \nabla_{\Gamma_h(t)} \chi_j(\mathbf{x}, t) \cdot \nabla_{\Gamma_h(t)} \chi_k(\mathbf{x}, t) d\mathbf{x},$$

$$\mathcal{I}(t)^j = \int_{\Gamma_h(t)} \chi_j(\mathbf{x}, t) d\mathbf{x},$$

$$\mathcal{F}(t)^j = f(\mathbf{x}, t).$$
(3.20)

Let U^n and V^n be N_p -dimensional column vectors for the solution ϕ_h^n and ψ_h^n , then the matrix forms of (3.11) and (3.12) respectively are

$$\begin{pmatrix}
\frac{1}{\Delta t}\mathcal{M}^{n+1} & M\mathcal{S}^{n+1} \\
-\epsilon \mathcal{S}^{n+1} - \frac{\beta}{\epsilon}\mathcal{M}^{n+1} & \mathcal{M}^{n+1}
\end{pmatrix} \begin{pmatrix} U^{n+1} \\ V^{n+1} \end{pmatrix}$$

$$= \begin{pmatrix}
\left(\frac{1}{\Delta t} - M\alpha\epsilon\right)\mathcal{M}^{n}U^{n} + \frac{M\alpha\epsilon}{|\Gamma_{h}^{n}|}\mathcal{M}^{n}\mathcal{I}^{n} \\
\frac{1}{\epsilon}\mathcal{M}^{n}\mathcal{F}^{n} - \frac{\beta}{\epsilon}\mathcal{M}^{n}U^{n}
\end{pmatrix}, (3.21)$$

and

$$\begin{pmatrix}
\frac{3}{2\Delta t}\mathcal{M}^{n+1} & M\mathcal{S}^{n+1} \\
-\epsilon \mathcal{S}^{n+1} - \frac{\beta \Delta t}{\epsilon}\mathcal{M}^{n+1} & \mathcal{M}^{n+1}
\end{pmatrix} \begin{pmatrix} U^{n+1} \\ V^{n+1} \end{pmatrix}$$

$$= \begin{pmatrix}
A \\
\frac{1}{\epsilon} (2\mathcal{M}^n \mathcal{F}^n - \mathcal{M}^{n-1} \mathcal{F}^{n-1}) - \frac{\beta \Delta t}{\epsilon} \mathcal{M}^n U^n
\end{pmatrix}, (3.22)$$

where

$$A = \left(-2M\alpha\epsilon + \frac{2}{\Delta t}\right)\mathcal{M}^n U^n + \left(M\alpha\epsilon - \frac{1}{2\Delta t}\right)\mathcal{M}^{n-1} U^{n-1} + \frac{2M\alpha\epsilon}{|\Gamma_h^n|}\mathcal{M}^n \mathcal{I}^n - \frac{M\alpha\epsilon}{|\Gamma_h^{n-1}|}\mathcal{M}^{n-1} \mathcal{I}^{n-1}.$$

4. Stability analysis

In this section, we show the stability of the numerical schemes (3.11) and (3.12) presented in the previous section. To facilitate the stability analysis while considering the simplicity the proof, we set $\beta=0$ in this study. The proof for $\beta>0$ needs more analytical skills and is elusive. Before formally gaining the stability conclusions, we first introduce some lemmas and estimates.

For the fully discretization, we analyze the L^2 -stability by assuming that the velocity is uniformly bounded as follows:

$$\left\|\nabla_{\Gamma_h(t)} \cdot v_h(\mathbf{x}, t)\right\|_{L^{\infty}(\Gamma_h(t))} \leqslant c,\tag{4.1}$$

constant c depends only on the surface velocity and is independent of model parameters.

Lemma 4.1 ([9]). Let $\theta_h^n \in S_h^n$, $\theta_h^{n+1} \in S_h^{n+1}$, to get

$$\frac{m_h(\theta_h^{n+1}, \theta_h^{n+1}) - m_h(\theta_h^n, \theta_h^n)}{\Delta t} - m_h(\theta_h^n, \partial_h^{\bullet} \theta_h^n)
= \frac{m_h(\theta_h^{n+1}, \theta_h^{n+1}) - m_h(\theta_h^n, \theta_h^n)}{2\Delta t} + \frac{1}{2} \Delta t m_h(\partial_h^{\bullet} \theta_h^n, \partial_h^{\bullet} \theta_h^n)
+ \frac{m_h(\theta_h^{n+1}, \theta_h^{n+1}) - m_h(\widetilde{\theta}_h^{n+1}(\cdot, t^n), \widetilde{\theta}_h^{n+1}(\cdot, t^n))}{2\Delta t},$$
(4.2)

where $\widetilde{\theta}_h^{n+1}(\cdot, t^n) = \theta_h^n + \Delta t \partial_h^{\bullet} \theta_h^n$.

Lemma 4.2 ([9]). *Under assumption* (4.1), the bilinear form has the following estimate:

$$\left| m_h \left(\theta_h^{n+1}, \theta_h^{n+1} \right) - m_h \left(\widetilde{\theta}_h^{n+1} (\cdot, t^n), \widetilde{\theta}_h^{n+1} (\cdot, t^n) \right) \right| \leqslant c \Delta t m_h \left(\theta_h^{n+1}, \theta_h^{n+1} \right), \tag{4.3}$$

where $\Delta t \leq \tau_0$, τ_0 and c are constants related to the model.

Assumption 4.1. In the CH phase-field model of the diblock copolymer, the nonlinear term is estimated as follows:

$$|f(\phi_h^n)| \leqslant L|\phi_h^n|,\tag{4.4}$$

where L is a constant.

When conducting stability analysis of the current scheme, it is unavoidable to make assumptions about the nonlinear term. This represents a limitation of the stabilized methods employed in the theoretical analysis. A common compromise is to modify the form of the nonlinear term to control its bound, as referenced in [33].

The following Hölder inequality is intended to deal with the term $m_h(\bar{\phi}_h^n, \eta_h^n)$.

Lemma 4.3. Suppose p>1 and 1/p+1/q=1. If $\mu_h^n(\mathbf{z},t)\in L^p(\Omega)$, $\upsilon_h^n(\mathbf{z},t)\in L^p(\Omega)$, then

$$\int_{\Omega} \mu_h^n(\mathbf{z}, t) \upsilon_h^n(\mathbf{z}, t) d\mathbf{z} \leqslant \left(\int_{\Omega} |\mu_h^n(\mathbf{z}, t)|^p \right)^{\frac{1}{p}} \left(\int_{\Omega} |\upsilon_h^n(\mathbf{z}, t)|^q \right)^{\frac{1}{q}}.$$
 (4.5)

In particular, if p=2, inequality (4.5) is applied, the estimate for term $m_h(\bar{\phi}_h^n, \phi_h^n)$ is as follows:

$$m_{h}(\bar{\phi}_{h}^{n}, \phi_{h}^{n}) = \frac{1}{|\Omega|} \int_{\Omega} \phi_{h}^{n} d\mathbf{z} \int_{\Omega} \phi_{h}^{n} d\mathbf{z}$$

$$\leq \frac{1}{|\Omega|} \left(\int_{\Omega} 1^{2} d\mathbf{z} \right)^{\frac{1}{2}} \left(\int_{\Omega} (\phi_{h}^{n})^{2} d\mathbf{z} \right)^{\frac{1}{2}} \left(\int_{\Omega} 1^{2} d\mathbf{z} \right)^{\frac{1}{2}} \left(\int_{\Omega} (\phi_{h}^{n})^{2} d\mathbf{z} \right)^{\frac{1}{2}}$$

$$= m_{h}(\phi_{h}^{n}, \phi_{h}^{n}). \tag{4.6}$$

Lemma 4.4. For $\Delta \hat{t} > 0$, $k \geqslant 0$, let $\hat{a}_k, \hat{b}_k, \hat{c}_k, \hat{d}_k$ and \bar{C} be nonnegative numbers, if

$$\hat{a}_r + \Delta \hat{t} \sum_{k=0}^r \hat{b}_k \leqslant \Delta \hat{t} \sum_{k=0}^{r-1} \hat{d}_k \hat{a}_k + \Delta \hat{t} \sum_{k=0}^{r-1} \hat{c}_k + \bar{C}, \quad \forall r \geqslant 1.$$
 (4.7)

Then

$$\hat{a}_r + \Delta \hat{t} \sum_{k=0}^r \hat{b}_k \leqslant \exp\left(\Delta \hat{t} \sum_{k=0}^{r-1} \hat{d}_k\right) \left(\Delta \hat{t} \sum_{k=0}^{r-1} \hat{c}_k + \bar{C}\right), \quad \forall r \geqslant 1.$$
 (4.8)

Lemma 4.4 is known as the discrete Gronwall Lemma [17, 32]. The following inequality

$$ab \leqslant \tau a^2 + \frac{1}{4\tau}b^2, \quad \forall \tau > 0 \tag{4.9}$$

will be used when dealing with nonlinear terms. The notation

$$\|\phi_h^n\|^2 = m_h^n (\phi_h^n, \phi_h^n)$$
 (4.10)

is to simplify writing.

Theorem 4.1. Let $\Delta t = T/N$ be the step size, satisfying $c\Delta t \leq 1/2$, where N is a positive integer, T represents the final time, and c is a constant associated with the model. For the CH phase-field model of the diblock copolymer, the fully discrete solution ϕ_h^n for the first-order semi-implicit scheme is bounded in L^2 -norm as follows:

$$(1 - c\Delta t) \|\phi_h^n\|^2 + (\Delta t)^2 \sum_{i=0}^{n-1} \|\partial_h^{\bullet} \phi_h^i\|^2 + \frac{2M\Delta t}{\epsilon} \|\psi_h^n\|^2$$

$$\leq e^{\frac{2c\epsilon^3 + ML^2}{2\epsilon^3} T} \left(\frac{M}{c\epsilon} \|\psi_h^0\|^2 + \|\phi_h^0\|^2 \right). \tag{4.11}$$

Proof. Let $\eta_h^{n+1}=\phi_h^{n+1}$, $\eta_h^n=\phi_h^n$, $\xi_h^{n+1}=\psi_h^{n+1}$, and by using Lemma 4.1, obtain

$$\begin{cases}
\frac{1}{2\Delta t} \left(m_h(\phi_h^{n+1}, \phi_h^{n+1}) - m_h(\phi_h^n, \phi_h^n) \right) \\
+ \frac{1}{2\Delta t} \left(m_h(\phi_h^{n+1}, \phi_h^{n+1}) - m_h(\widetilde{\phi}_h^{n+1}(\cdot, t^n), \widetilde{\phi}_h^{n+1}(\cdot, t^n)) \right) \\
+ \frac{1}{2} \Delta t m_h(\partial_h^{\bullet} \phi_h^n, \partial_h^{\bullet} \phi_h^n) + M a_h(\psi_h^{n+1}, \phi_h^{n+1}) \\
+ M \alpha \epsilon \left(m_h(\phi_h^n, \phi_h^n) - m_h(\bar{\phi}_h^n, \phi_h^n) \right) = 0, \\
m_h(\psi_h^{n+1}, \psi_h^{n+1}) = \epsilon a_h(\phi_h^{n+1}, \psi_h^{n+1}) + \frac{1}{\epsilon} m_h(f(\phi_h^n), \psi_h^n).
\end{cases} (4.12)$$

Using Lemma 4.2 and merging equations, we get

$$\frac{1}{2\Delta t} \left(m_h(\phi_h^{n+1}, \phi_h^{n+1}) - m_h(\phi_h^n, \phi_h^n) \right) + \frac{1}{2} \Delta t m_h \left(\partial_h^{\bullet} \phi_h^n, \partial_h^{\bullet} \phi_h^n \right)
+ \frac{M}{\epsilon} m_h \left(\psi_h^{n+1}, \psi_h^{n+1} \right) - \frac{M}{\epsilon^2} m_h \left(f(\phi_h^n), \psi_h^n \right)
+ M \alpha \epsilon \left(m_h(\phi_h^n, \phi_h^n) - m_h(\bar{\phi}_h^n, \phi_h^n) \right)
\leqslant \frac{c}{2} m_h \left(\phi_h^{n+1}, \phi_h^{n+1} \right).$$
(4.13)

Using Eq. (4.9) and Lemma 4.3 to deal with the nonlinear term and the term $m_h(\phi_h^n, \phi_h^n) - m_h(\bar{\phi}_h^n, \bar{\phi}_h^n)$, we obtain that

$$\frac{1}{2\Delta t} \left(m_h(\phi_h^{n+1}, \phi_h^{n+1}) - m_h(\phi_h^n, \phi_h^n) \right) + \frac{1}{2} \Delta t m_h \left(\partial_h^{\bullet} \phi_h^n, \partial_h^{\bullet} \phi_h^n \right)
+ \frac{M}{\epsilon} m_h \left(\psi_h^{n+1}, \psi_h^{n+1} \right)
\leqslant \frac{c}{2} m_h \left(\phi_h^{n+1}, \phi_h^{n+1} \right) + \frac{M}{\epsilon^2} \left(\frac{1}{4\epsilon} m_h \left(f(\phi_h^n), f(\phi_h^n) \right) + \epsilon m_h(\psi_h^n, \psi_h^n) \right).$$
(4.14)

Summing the above equation from 0 to n-1, we get

$$\frac{1}{2\Delta t} \left(m_h(\phi_h^n, \phi_h^n) - m_h(\phi_h^0, \phi_h^0) \right) + \frac{1}{2} \Delta t \sum_{i=0}^{n-1} m_h \left(\partial_h^{\bullet} \phi_h^i, \partial_h^{\bullet} \phi_h^i \right) \\
+ \frac{M}{\epsilon} \left(m_h(\psi_h^n, \psi_h^n) - m_h(\psi_h^0, \psi_h^0) \right) \\
\leqslant \frac{c}{2} \sum_{i=1}^{n} m_h \left(\phi_h^i, \phi_h^i \right) + \frac{M}{4\epsilon^3} \sum_{i=0}^{n-1} m_h \left(f(\phi_h^i), f(\phi_h^i) \right). \tag{4.15}$$

Using Assumption 4.1 and Eq. (4.10), we obtain

$$\frac{1}{2\Delta t} (\|\phi_h^n\|^2 - \|\phi_h^0\|^2) + \frac{1}{2}\Delta t \sum_{i=0}^{n-1} \|\partial_h^{\bullet} \phi_h^i\|^2 + \frac{M}{\epsilon} (\|\psi_h^n\|^2 - \|\psi_h^0\|^2)$$

$$\leq \frac{c}{2} \sum_{i=1}^{n} \|\phi_h^i\|^2 + \frac{ML^2}{4\epsilon^3} \sum_{i=0}^{n-1} \|\phi_h^i\|^2.$$
 (4.16)

By multiplying both sides by $2\Delta t$ and simplifying, we arrive at the result

$$(1 - c\Delta t)\|\phi_h^n\|^2 + (\Delta t)^2 \sum_{i=0}^{n-1} \|\partial_h^{\bullet} \phi_h^i\|^2 + \frac{2M\Delta t}{\epsilon} \|\psi_h^n\|^2$$

$$\leq \left(c + \frac{ML^2}{2\epsilon^3}\right) \Delta t \sum_{i=1}^{n-1} \|\phi_h^i\|^2 + \frac{2M\Delta t}{\epsilon} \|\psi_h^0\|^2 + \|\phi_h^0\|^2. \tag{4.17}$$

Applying inequality $n\Delta t \leqslant N\Delta t = T$ and Lemma 4.4, we have

$$(1 - c\Delta t) \|\phi_h^n\|^2 + (\Delta t)^2 \sum_{i=0}^{n-1} \|\partial_h^{\bullet} \phi_h^i\|^2 + \frac{2M\Delta t}{\epsilon} \|\psi_h^n\|^2$$

$$\leq e^{\frac{2c\epsilon^3 + ML^2}{2\epsilon^3} T} \left(\frac{M}{c\epsilon} \|\psi_h^0\|^2 + \|\phi_h^0\|^2 \right), \tag{4.18}$$

which is the proof for the Theorem 4.1.

Theorem 4.2. Assume that N is a positive integer and T represents the eventual moment. Let $\Delta t = T/N$ be the time step, which satisfies the condition $2c\Delta t \leq 1/2$, where c is a constant that depends on the model. For the CH phase-field model of the diblock copolymer, the fully discrete solution ϕ_h^n for the second-order semi-implicit scheme is bounded in L^2 -norm as follows:

$$(1 - 2c\Delta t)\|\phi_h^n\|^2 + (\Delta t)^2 \sum_{i=1}^{n-1} \|\partial_h^{\bullet} \phi_h^i\|^2 + \frac{2M\Delta t}{\epsilon} \|\psi_h^n\|^2$$

$$\leq e^{\frac{6c\epsilon^3 + 9ML^2}{2\epsilon^3} T} \left(\frac{M\alpha\epsilon}{2c} \|\phi_h^0\|^2 + \|\phi_h^1\|^2 + \frac{1}{16c^2} \|\partial_h^{\bullet} \phi_h^0\|^2 + \frac{M}{2c\epsilon} \|\psi_h^1\|^2 \right). \tag{4.19}$$

Proof. Let

$$\begin{split} & \eta_h^{n+1} = \phi_h^{n+1}, \quad \eta_h^n = \phi_h^n, \quad \eta_h^{n-1} = \phi_h^{n-1}, \\ & \xi_h^{n+1} = \psi_h^{n+1}, \quad \xi_h^n = \psi_h^n, \quad \xi_h^{n-1} = \psi_h^{n-1}. \end{split}$$

Combining the two equations, we have

$$\frac{1}{\Delta t} \left(m_h(\phi_h^{n+1}, \phi_h^{n+1}) - m_h(\phi_h^n, \phi_h^n) \right) - 2m_h \left(\phi_h^n, \partial_h^{\bullet} \phi_h^n \right) \\
- \left(\frac{1}{2\Delta t} \left(m_h(\phi_h^n, \phi_h^n) - m_h(\phi_h^{n-1}, \phi_h^{n-1}) \right) - m_h \left(\phi_h^{n-1}, \partial_h^{\bullet} \phi_h^{n-1} \right) \right) \\
+ \frac{1}{2\Delta t} \left(m_h(\phi_h^{n+1}, \phi_h^{n+1}) - m_h(\phi_h^n, \phi_h^n) \right) + \frac{M}{\epsilon} m_h \left(\psi_h^{n+1}, \psi_h^{n+1} \right)$$

$$-\frac{M}{\epsilon^{2}} \left(2m_{h} \left(f(\phi_{h}^{n}), \psi_{h}^{n} \right) - m_{h} \left(f(\phi_{h}^{n-1}), \psi_{h}^{n-1} \right) \right)$$

$$+ 2M\alpha \epsilon \left(m_{h} (\phi_{h}^{n}, \phi_{h}^{n}) - m_{h} (\bar{\phi}_{h}^{n}, \phi_{h}^{n}) \right)$$

$$- M\alpha \epsilon \left(m_{h} (\phi_{h}^{n-1}, \phi_{h}^{n-1}) - m_{h} (\bar{\phi}_{h}^{n-1}, \phi_{h}^{n-1}) \right) = 0.$$
(4.20)

Using Lemma 4.1, we obtain

$$\frac{1}{2\Delta t} \left(m_h(\phi_h^{n+1}, \phi_h^{n+1}) - m_h(\phi_h^n, \phi_h^n) \right) + \Delta t m_h \left(\partial_h^{\bullet} \phi_h^n, \partial_h^{\bullet} \phi_h^n \right)
+ \frac{1}{\Delta t} \left(m_h(\phi_h^{n+1}, \phi_h^{n+1}) - m_h(\widetilde{\phi}_h^n(\cdot, t^n), \widetilde{\phi}_h^n(\cdot, t^n)) \right) - \frac{1}{2} \Delta t m_h \left(\partial_h^{\bullet} \phi_h^{n-1}, \partial_h^{\bullet} \phi_h^{n-1} \right)
- \frac{1}{2\Delta t} \left(m_h(\phi_h^n, \phi_h^n) - m_h(\widetilde{\phi}_h^n(\cdot, t^{n-1}), \widetilde{\phi}_h^n(\cdot, t^{n-1})) \right)
+ \frac{M}{\epsilon} m_h \left(\psi_h^{n+1}, \psi_h^{n+1} \right) - \frac{M}{\epsilon^2} \left(2 m_h \left(f(\phi_h^n), \psi_h^n \right) - m_h \left(f(\phi_h^{n-1}), \psi_h^{n-1} \right) \right)
+ 2 M \alpha \epsilon \left(m_h(\phi_h^n, \phi_h^n) - m_h(\overline{\phi}_h^n, \phi_h^n) \right)
- M \alpha \epsilon \left(m_h(\phi_h^{n-1}, \phi_h^{n-1}) - m_h(\overline{\phi}_h^{n-1}, \phi_h^{n-1}) \right) = 0.$$
(4.21)

Applying Lemma 4.2, we have

$$\frac{1}{2\Delta t} \left(m_h(\phi_h^{n+1}, \phi_h^{n+1}) - m_h(\phi_h^n, \phi_h^n) \right) + \Delta t m_h \left(\partial_h^{\bullet} \phi_h^n, \partial_h^{\bullet} \phi_h^n \right) \\
- \frac{1}{2} \Delta t m_h \left(\partial_h^{\bullet} \phi_h^{n-1}, \partial_h^{\bullet} \phi_h^{n-1} \right) + \frac{M}{\epsilon} m_h \left(\psi_h^{n+1}, \psi_h^{n+1} \right) \\
+ 2M \alpha \epsilon \left(m_h (\phi_h^n, \phi_h^n) - m_h (\bar{\phi}_h^n, \phi_h^n) \right) \\
- M \alpha \epsilon \left(m_h (\phi_h^{n-1}, \phi_h^{n-1}) - m_h (\bar{\phi}_h^{n-1}, \phi_h^{n-1}) \right) \\
\leqslant c m_h \left(\phi_h^{n+1}, \phi_h^{n+1} \right) + \frac{c}{2} m_h \left(\phi_h^n, \phi_h^n \right) \\
+ \frac{M}{\epsilon^2} \left(2 m_h (f(\phi_h^n), \psi_h^n) - m_h (f(\phi_h^{n-1}), \psi_h^{n-1}) \right). \tag{4.22}$$

Summing the Eq. (4.22) from 1 to n-1 and performing simplification, we get

$$\frac{1}{2\Delta t} \left(m_h(\phi_h^n, \phi_h^n) - m_h(\phi_h^1, \phi_h^1) \right) + \frac{1}{2} \Delta t \sum_{i=1}^{n-1} m_h(\partial_h^{\bullet} \phi_h^i, \partial_h^{\bullet} \phi_h^i)
+ \frac{M}{\epsilon} \sum_{i=2}^n m_h(\psi_h^i, \psi_h^i) + M\alpha \epsilon \sum_{i=1}^{n-1} \left(m_h(\phi_h^i, \phi_h^i) - m_h(\bar{\phi}_h^i, \phi_h^i) \right)
+ M\alpha \epsilon \left(m_h(\phi_h^{n-1}, \phi_h^{n-1}) - m_h(\bar{\phi}_h^{n-1}, \phi_h^{n-1}) \right)
\leqslant c \sum_{i=2}^n m_h(\phi_h^i, \phi_h^i) + \frac{c}{2} \sum_{i=1}^{n-1} m_h(\phi_h^i, \phi_h^i)
+ M\alpha \epsilon \left(m_h(\phi_h^0, \phi_h^0) - m_h(\bar{\phi}_h^0, \phi_h^0) \right) + \frac{1}{2} \Delta t m_h(\partial_h^{\bullet} \phi_h^0, \partial_h^{\bullet} \phi_h^0)$$

$$+ \frac{M}{\epsilon^2} \left(\sum_{i=1}^{n-1} m_h \left(f(\phi_h^i), \psi_h^i \right) + m_h \left(f(\phi_h^{n-1}), \psi_h^{n-1} \right) - m_h \left(f(\phi_h^0), \psi_h^0 \right) \right).$$
 (4.23)

Using inequality (4.9) (let $\tau = \epsilon/3$) and Lemma 4.3, we have

$$\frac{1}{2\Delta t} \left(m_h(\phi_h^n, \phi_h^n) - m_h(\phi_h^1, \phi_h^1) \right) + \frac{1}{2} \Delta t \sum_{i=1}^{n-1} m_h \left(\partial_h^{\bullet} \phi_h^i, \partial_h^{\bullet} \phi_h^i \right) + \frac{M}{\epsilon} \sum_{i=2}^n m_h \left(\psi_h^i, \psi_h^i \right) \\
\leqslant c \sum_{i=2}^n m_h \left(\phi_h^i, \phi_h^i \right) + \frac{c}{2} \sum_{i=1}^{n-1} m_h \left(\phi_h^i, \phi_h^i \right) + M \alpha \epsilon m_h \left(\phi_h^0, \phi_h^0 \right) + \frac{1}{2} \Delta t m_h \left(\partial_h^{\bullet} \phi_h^0, \partial_h^{\bullet} \phi_h^0 \right) \\
+ \frac{3M}{\epsilon^2} \left(\frac{3}{4\epsilon} \sum_{i=1}^{n-1} m_h \left(f(\phi_h^i), f(\phi_h^i) \right) + \frac{\epsilon}{3} \sum_{i=1}^{n-1} m_h (\psi_h^i, \psi_h^i) \right). \tag{4.24}$$

Using Assumption 4.1 and Eq. (4.10), we get

$$\frac{1}{2\Delta t} (\|\phi_h^n\|^2 - \|\phi_h^1\|^2) + \frac{1}{2}\Delta t \sum_{i=1}^{n-1} \|\partial_h^{\bullet} \phi_h^i\|^2 + \frac{M}{\epsilon} \left(\sum_{i=2}^n \|\psi_h^i\|^2 - \sum_{i=1}^{n-1} \|\psi_h^i\|^2 \right) \\
\leqslant c \sum_{i=2}^n \|\phi_h^i\|^2 + \frac{c}{2} \sum_{i=1}^{n-1} \|\phi_h^i\|^2 + M\alpha \epsilon \|\phi_h^0\|^2 + \frac{1}{2}\Delta t \|\partial_h^{\bullet} \phi_h^0\|^2 + \frac{9ML^2}{4\epsilon^3} \sum_{i=1}^{n-1} \|\phi_h^i\|^2.$$
(4.25)

Multiplying both sides of above equation by $2\Delta t$ and performing simplification, we have

$$(1 - 2c\Delta t)\|\phi_{h}^{n}\|^{2} + (\Delta t)^{2} \sum_{i=1}^{n-1} \|\partial_{h}^{\bullet}\phi_{h}^{i}\|^{2} + \frac{2M\Delta t}{\epsilon} \|\psi_{h}^{n}\|^{2}$$

$$\leq \left(3c + \frac{9ML^{2}}{2\epsilon^{3}}\right) \Delta t \sum_{i=0}^{n-1} \|\phi_{h}^{i}\|^{2} + 2M\alpha\epsilon\Delta t \|\phi_{h}^{0}\|^{2} + \|\phi_{h}^{1}\|^{2}$$

$$+ (\Delta t)^{2} \|\partial_{h}^{\bullet}\phi_{h}^{0}\|^{2} + \frac{2M\Delta t}{\epsilon} \|\psi_{h}^{1}\|^{2}. \tag{4.26}$$

Applying Lemma 4.4 and inequality $n\Delta t \leq N\Delta t = T$, we get

$$(1 - 2c\Delta t)\|\phi_h^n\|^2 + (\Delta t)^2 \sum_{i=1}^{n-1} \|\partial_h^{\bullet} \phi_h^i\|^2 + \frac{2M\Delta t}{\epsilon} \|\psi_h^n\|^2$$

$$\leq e^{\frac{6c\epsilon^3 + 9ML^2}{2\epsilon^3} T} \left(\frac{M\alpha \epsilon}{2c} \|\phi_h^0\|^2 + \|\phi_h^1\|^2 + \frac{1}{16c^2} \|\partial_h^{\bullet} \phi_h^0\|^2 + \frac{M}{2c\epsilon} \|\psi_h^1\|^2 \right), \tag{4.27}$$

which is the second-order stability analysis.

Let

$$\mathcal{G}_1 := \frac{2c\epsilon^3 + ML^2}{2\epsilon^3}, \quad \mathcal{G}_2 := \frac{6c\epsilon^3 + 9ML^2}{2\epsilon^3}$$

be the growth factors. It is important to note that the constant c depends solely on the surface velocity, allowing us to select a relatively large time step size to ensure that $1-2c\Delta t\geqslant 0$. However, given the large magnitude of \mathcal{G}_1 and \mathcal{G}_2 , which is of order $\mathcal{O}(1/\epsilon^3)$, there is a significant risk of numerical instability or divergence when setting $\Delta t=\mathcal{O}(1)$. Our main objective is to bolster stability by incorporating linear stabilization terms. Based on our experience on the stability analysis of the Allen-Cahn equation on the evolving surface, it can be expect that the growth factors can be reduced to $\mathcal{O}(1/(\epsilon^3+\beta\Delta t))$, indicating superior stability when the stabilized coefficient is higher. However, it is important to note that extremely large β values may compromise accuracy. After conducting extensive numerical testing, we selected a stabilized parameter β within the range of 6 to 8 for our study.

5. Numerical simulation

Numerical experiments are performed in this section to exhibit the convergence, mass evolution and stability of the SSI scheme. Additionally, the behavior of CH model of diblock copolymers on evolving surfaces is investigated.

5.1. Test of convergence

We display the orders of the convergence for the proposed model. The H^1 - and L^2 -errors are considered. We choose the parameters $\epsilon=1,\ \beta=6,\ \alpha=1,\ T_0=0,\ T=0.1,\ M=1,$ take

$$v(\mathbf{x},t) = \boldsymbol{n}(\mathbf{x},t)$$

as the velocity, and conduct the experiment on the surface

$$\Gamma(\mathbf{x},t) = x^2 + y^2 + z^2 - (0.5 + t)^2,$$

where $n(\mathbf{x},t)$ is the unit outer normal vector of the surface. The time steps are $\Delta t = h^2$ and $\Delta t = 0.1h$ for the first-order and second-order schemes, respectively. We set the exact solution as

$$\phi(\mathbf{x}, t) = e^{-t} \sin(\pi x y z^2).$$

The errors and convergence orders are shown in Fig. 2.

5.2. Test of the stability

In this subsection, we display the stability of presented numerical scheme. As previously stated, the stabilized term plays an essential role in maintaining numerical simulation stability for a long time. Therefore, we will test whether the stabilized term has a positive effect on the numerical simulation.

The initial value is set to be

$$\phi^0({\bf x},t) = 0.05 {\rm rand},$$

where rand is a random value in [-1,1]. In order to compare the effect of the stabilized terms on stability, the initial value is the same for the experiment with different stabilized coefficients. The parameters are $\epsilon=0.025$, $\alpha=20000$, h=0.0512, $\Delta t=0.005$, M=1. The evolving surface is chosen to be

$$\Gamma(\mathbf{x},t) = x^2 + y^2 + z^2 - (0.6 + 0.15\sin(2\pi t))^2$$

with the velocity

$$v(\mathbf{x}, t) = 0.3\pi \cos(2\pi t) \mathbf{n}(\mathbf{x}, t).$$

The numerical simulation with $\beta=8$ performs well, as can be seen from the findings in Fig. 3. When $\beta=0$, the numerical solution blows up after a few time steps. This can lead to the conclusion that the algorithm with the stabilized term is more stable than the algorithm without stabilized term, that is, the SSI method is effective.

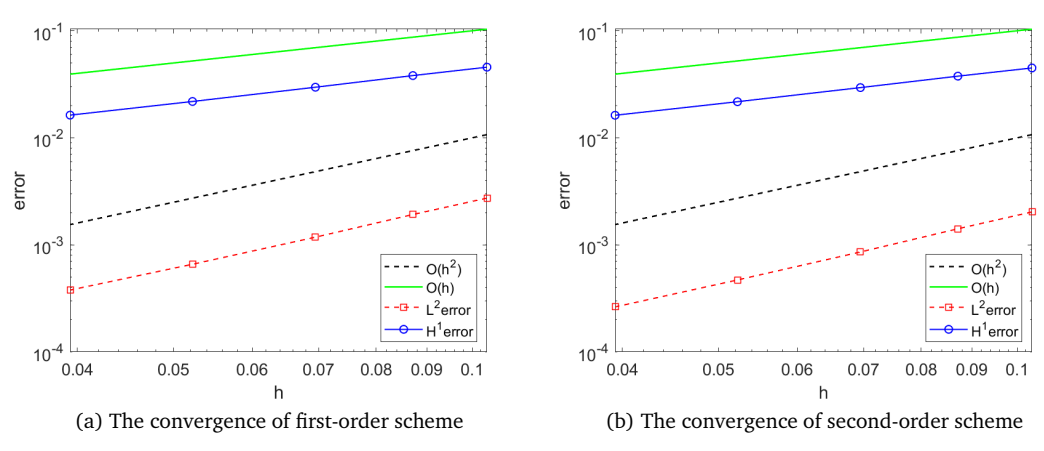


Figure 2: The convergence orders of the numerical method.

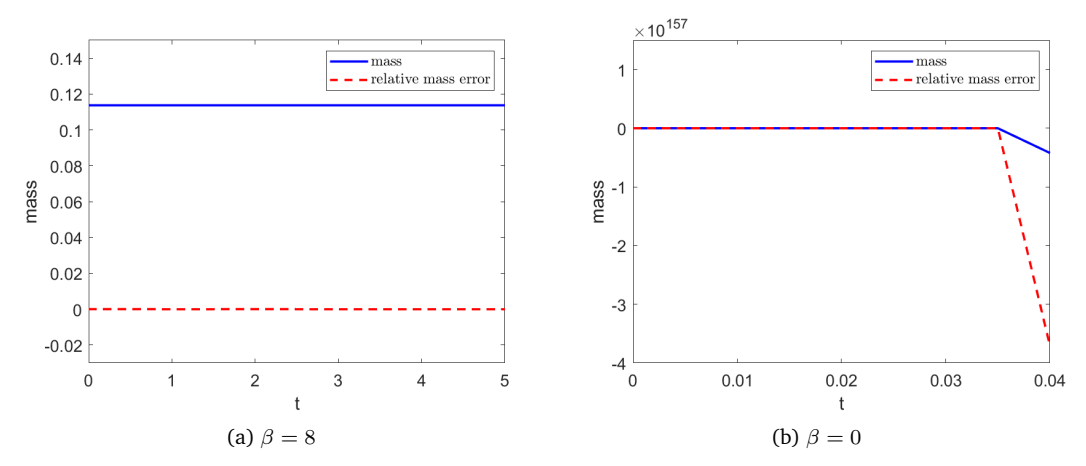


Figure 3: Comparison of numerical methods with and without stabilized term.

5.3. Spinodal decomposition and evolution of mass

This part researches the dynamics and mass evolution of the proposed model through some experiments on different evolving surfaces.

Experiments are performed on a sphere with a first-order scheme. The initial value is set to

$$\phi^0(\mathbf{x}, t) = \overline{\phi}_0 + 0.05 \text{rand.} \tag{5.1}$$

In this part, all initial values are according to (5.1). The evolving surface is

$$\Gamma(\mathbf{x},t) = x^2 + y^2 + z^2 - (2.2 + 0.25\sin(2\pi t))^2$$
(5.2)

with the velocity

$$v(\mathbf{x},t) = 0.5\pi \cos(2\pi t) \mathbf{n}(\mathbf{x},t). \tag{5.3}$$

The other parameters are $\epsilon=0.025,\,\beta=6,\,\alpha=20000,\,h=0.0525,\,\Delta t=0.005,\,M=1.$ The process of the spinodal decomposition is shown in Figs. 4-5.

We also conduct experiments to investigate the mass evolution and spinodal decomposition using the second-order scheme. The parameters are set to $\epsilon=0.025$, $\alpha=20000$, $\beta=6$, h=0.0271, $\Delta t=0.002$, M=0.0025. The process of spinodal decomposition will evolve on the evolving surface with the initial surface

$$\Gamma(\mathbf{x}) = (1 - \sqrt{x^2 + y^2})^2 + z^2 - 0.3^2,$$
 (5.4)

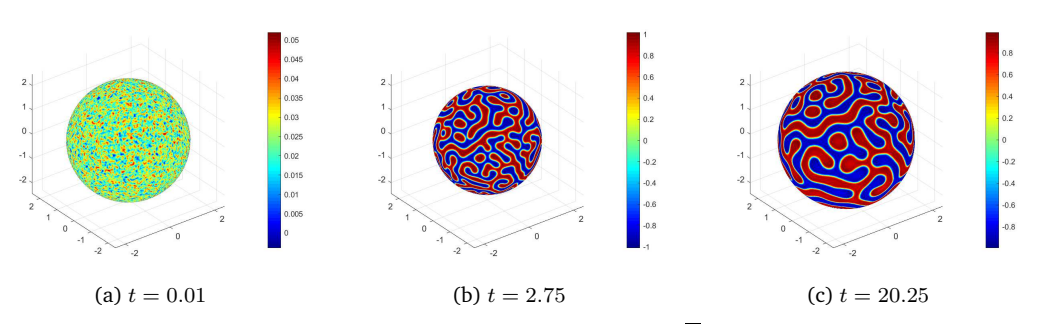


Figure 4: Spinodal decomposition with $\overline{\phi}$ =0.

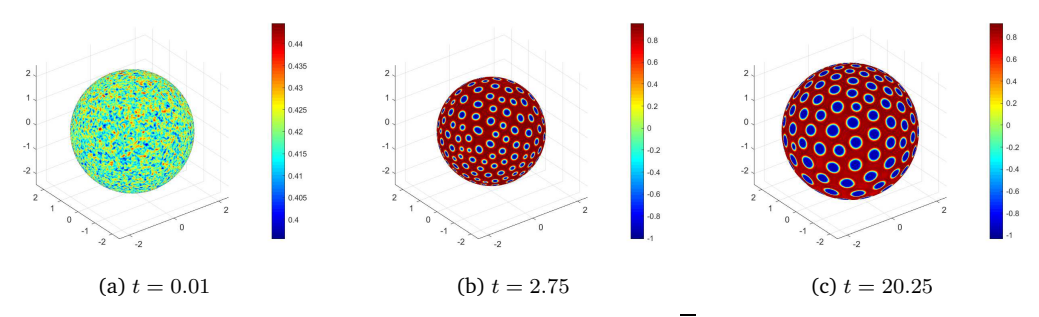


Figure 5: Spinodal decomposition with $\overline{\phi}$ =0.4.

and the velocity

$$v(\mathbf{x},t) = 0.008\phi \mathbf{n}(\mathbf{x},t). \tag{5.5}$$

Figs. 6-8 show the mass evolution and phase separation phenomena, respectively.

We further confirm that the mass error is smaller when the mesh is finer. We take two different mesh sizes 0.0523 and 0.0312 for comparison. The initial surface and the velocity are chosen with reference to Eqs. (5.4) and (5.5). The other parameters are $\epsilon=0.05,~\alpha=20000,~\beta=6,~\Delta t=0.001,$ and M=0.005. The plots in Fig. 9 indicate the desired result.

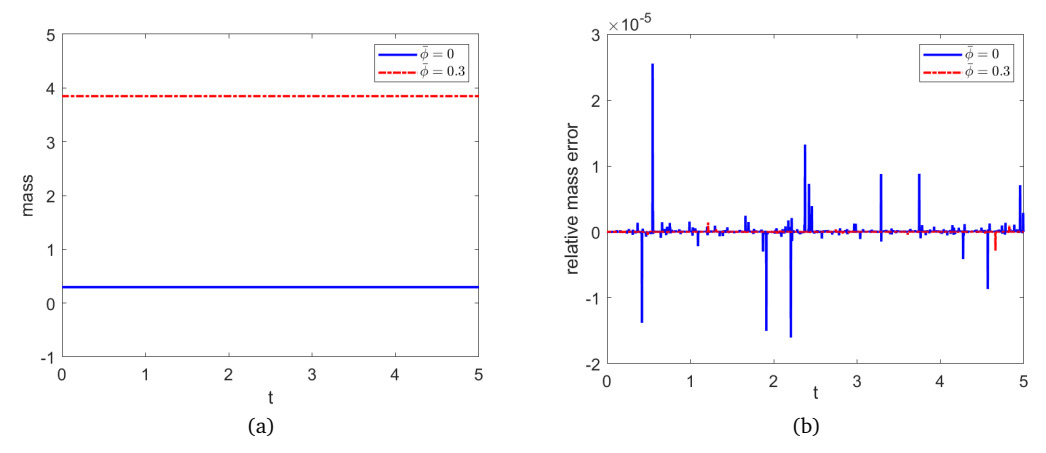


Figure 6: (a) The evolution of the mass. (b) The relative mass error.

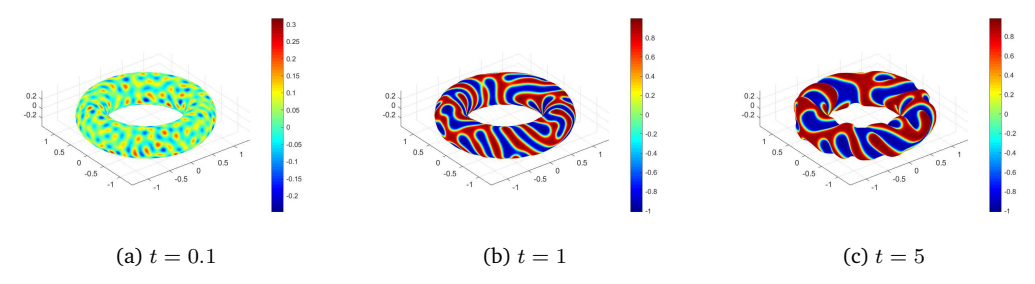


Figure 7: Spinodal decomposition with $\overline{\phi}$ =0.

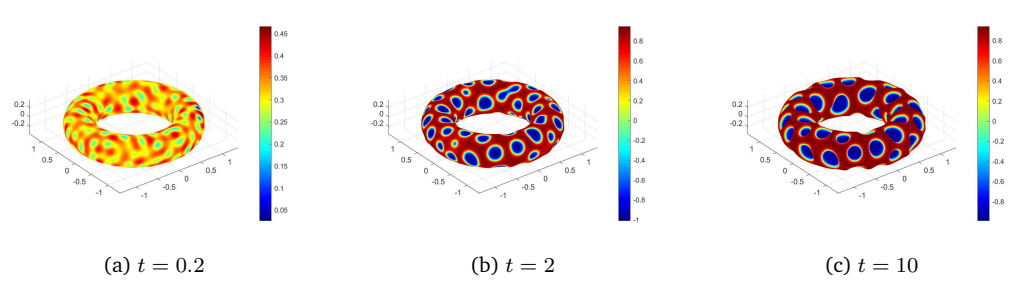


Figure 8: Spinodal decomposition with $\overline{\phi}$ =0.3.

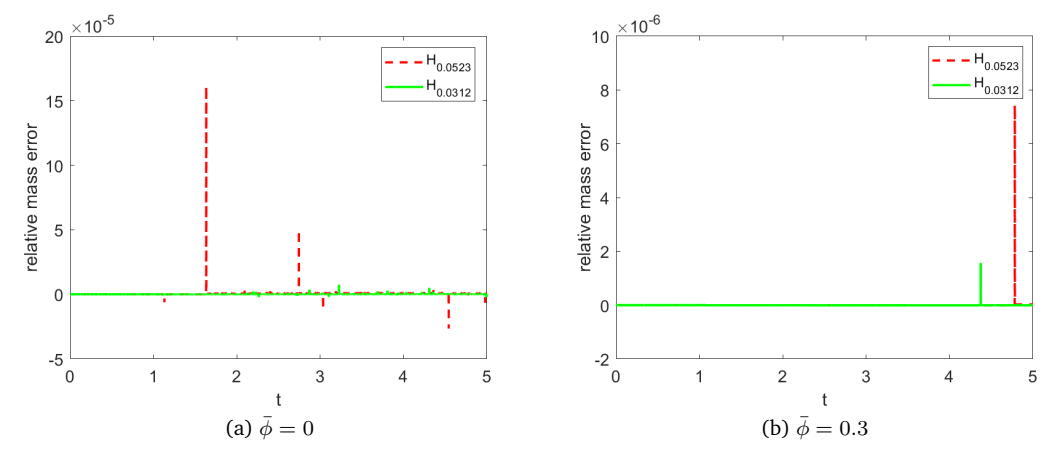


Figure 9: Comparison of errors of big and small discrete dimensions.

For the diversity of experiments, we perform experiments on different surfaces and get similar phenomena. The parameters are set to $\epsilon=0.025,~\alpha=20000,~\beta=6,~h=0.0405,~\Delta t=0.0025,~M=0.002$. The process of spinodal decomposition will evolve on the evolving surface with the initial surface

$$\Gamma(\mathbf{x}) = (1 + 4x^2)(1 + 4y^2)(1 + 4z^2) + 64xyz + 4x^2 + 4y^2 + 4z^2 - 6,$$
 (5.6)

and the velocity

$$v(\mathbf{x},t) = 0.005\phi \mathbf{n}(\mathbf{x},t). \tag{5.7}$$

The results of the experiment are shown in Figs. 10 and 11. Some conclusions can be drawn from the performance of these experiments. From Fig. 6, we can see that our model and algorithm satisfy the mass conservation property. Different phase separation experiments present the following conclusion. When we set $\overline{\phi}_0=0$, which indicates that the concentrations of the two blocks are approximately equal, the surface shows a process of striped changes. When $\overline{\phi}_0=0.3$ or 0.4, it indicates that the two block concentrations have a large difference, and the surface will appear to be a point-shaped evolution process.

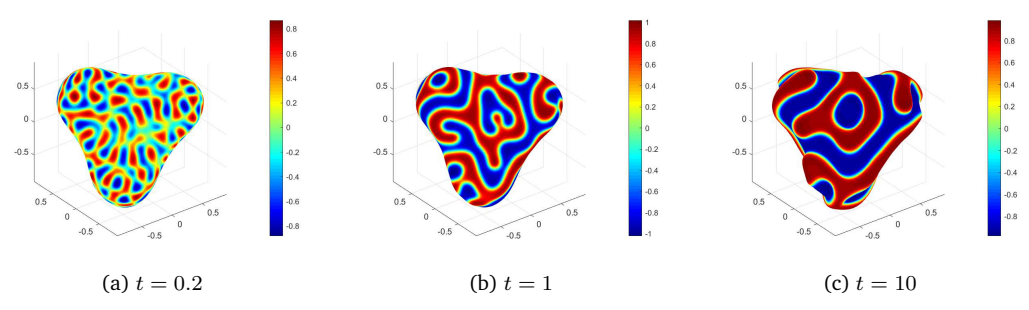


Figure 10: Spinodal decomposition with $\overline{\phi}$ =0.

In addition, we test on a rabbit-shaped surface that our model and method are also applicable to surfaces with large curvature. We chose the following parameters: S=6, $\epsilon=0.025,~M=0.005,~\alpha=20000,~\Delta t=0.001,~H=0.0248.$ The velocity is

$$v(\mathbf{x}, t) = 0.06[-y, x, 0] + 0.008\sin(t)\mathbf{n}(\mathbf{x}, t).$$
(5.8)

The result of spinodal decomposition can be seen in Fig. 12.

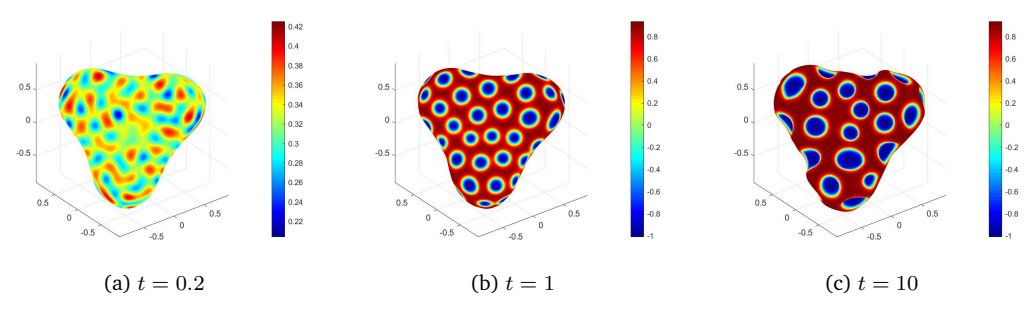


Figure 11: Spinodal decomposition with $\overline{\phi}$ =0.3.

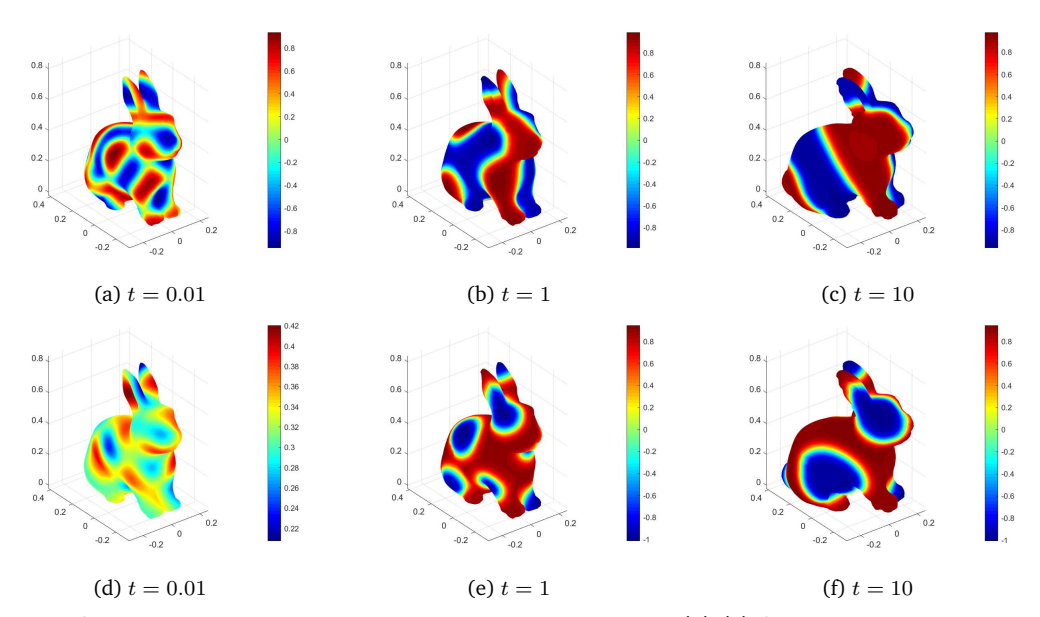


Figure 12: Spinodal decomposition on surfaces with large curvature. (a)-(c) Spinodal decomposition with $\overline{\phi}$ =0. (d)-(f) Spinodal decomposition with $\overline{\phi}$ =0.3.

6. Conclusion

In this work, we explore the CH phase-field model of diblock copolymers on evolving surfaces. The main work is to establish the CH model of diblock copolymers on

evolving surfaces and to design an efficient numerical algorithm for the model. The mass conservation property of the proposed model on evolving surfaces is preserved, as well as briefly proved. To achieve a numerical method that is linear, highly accurate, and stable, the stabilized semi-implicit approach is incorporated into the ESFEM. Theoretically, we analyze the first- and second-order stability results of the numerical method. Extensive numerical experiments explore the performance of CH model of diblock copolymers on evolving surfaces. We test the convergence of the model, evaluate the stability of the SSI scheme, demonstrate the mass conservation property, and show the spinodal decomposition process. In future research, we intend to conduct a deeper exploration of the error analysis related to our proposed numerical method. In addition, we also consider extending the CH model of diblock copolymers on evolving surfaces to N-component systems by coupling N equations.

Acknowledgements

The authors would like to thank the editor and referees for their valuable comments and suggestions which helped us to improve the results of this paper.

This work is supported by the National Natural Science Foundation of China (Grant Nos. 12361090, 12071406, 12271465), by the Natural Science Foundation of Xinjiang Province (Grant Nos. 2023D01C164, 2023D14014, 2022D01D32), and by the Tianshan Talent Training Program (Grant Nos. 2023TSYCQNTJ0015, 2022TSYCTD0019).

References

- [1] V. AGRAHARI AND V. AGRAHARI, Advances and applications of block-copolymer-based nanoformulations, Drug Discov. Today 23(5) (2018), 1139–1151.
- [2] G. A. Buxton and A. C. Balazs, Simulating the morphology and mechanical properties of filled diblock copolymers, Phys. Rev. E 67(3) (2003), 031802.
- [3] C. Chen, X. Li, J. Zhang, and X. Yang, Efficient linear, decoupled, and unconditionally stable scheme for a ternary Cahn-Hilliard type Nakazawa-Ohta phase-field model for triblock copolymers, Appl. Math. Comput. 388 (2021), 125463.
- [4] Q. Cheng, X. Yang, and J. Shen, Efficient and accurate numerical schemes for a hydro-dynamically coupled phase field diblock copolymer model, J. Comput. Phys. 341 (2017), 44–60.
- [5] X. Cheng, On the Stability of a Semi-Implicit Scheme of Cahn-Hilliard Type Equations, University of British Columbia, Theses, 2017.
- [6] R. CHOKSI, M. A. PELETIER, AND J. F. WILLIAMS, On the phase diagram for microphase separation of diblock copolymers: An approach via a nonlocal Cahn-Hilliard functional, SIAM J. Appl. Math. 69(6) (2009), 1712–1738.
- [7] J. DIAZ, M. PINNA, A. V. ZVELINDOVSKY, AND I. PAGONABARRAGA, *Phase behavior of block copolymer nanocomposite systems*, Adv. Theory Simul. 1(9) (2018), 1800066.
- [8] G. DZIUK AND C. M. ELLIOTT, Finite elements on evolving surfaces, IMA J. Numer. Anal. 27(2) (2007), 262–292.
- [9] G. DZIUK AND C. M. ELLIOTT, A fully discrete evolving surface finite element method, SIAM J. Numer. Anal. 50(5) (2012), 2677–2694.

- [10] G. DZIUK AND C. M. ELLIOTT, Finite element methods for surface PDEs, Acta Numer. 22 (2013), 289–396.
- [11] C. M. ELLIOTT AND T. RANNER, Evolving surface finite element method for the Cahn-Hilliard equation, Numer. Math. 129(3) (2015), 483–534.
- [12] X. FENG, T. TANG, AND J. YANG, Stabilized Crank-Nicolson/Adams-Bashforth schemes for phase field models, East Asian J. Appl. Math. 3(1) (2013), 59–80.
- [13] H. GARCKE, J. KAMPMANN, A. RÄTZ, AND M. RÖGER, A coupled surface-Cahn-Hilliard bulk-diffusion system modeling lipid raft formation in cell membranes, Math. Models Methods Appl. Sci. 26(06) (2016), 1149–1189.
- [14] B. J. GROSS, P. KUBERRY, AND P. J. ATZBERGER, First-passage time statistics on surfaces of general shape: Surface PDE solvers using Generalized Moving Least Squares (GMLS), J. Comput. Phys. 453 (2022), 110932.
- [15] B. J. GROSS, N. TRASK, P. KUBERRY, AND P. J. ATZBERGER, Meshfree methods on manifolds for hydrodynamic flows on curved surfaces: A generalized moving least-squares (GMLS) approach, J. Comput. Phys. 409 (2020), 109340.
- [16] E. HARTMANN, Geometry and Algorithms for Computer Aided Design, Darmstadt University of Technology, 2003.
- [17] Y. HE, A fully discrete stabilized finite-element method for the time-dependent Navier-Stokes problem, IMA J. Numer. Anal. 23(4) (2003), 665–691.
- [18] Y. HE, Y. LIU, AND T. TANG, *On large time-stepping methods for the Cahn-Hilliard equation*, Appl. Numer. Math. 57(5-7) (2007), 616–628.
- [19] S. Huang, X. Xiao, and X. Feng, An adaptive time-stepping method for the binary fluid-surfactant phase field model on evolving surfaces, J. Sci. Comput. 95(1) (2023), 29.
- [20] S. Huang, X. Xiao, and X. Feng, An adaptive time-stepping method for the phase-field molecular beam epitaxial growth model on evolving surfaces, Appl. Math. Comput. 439 (2023), 127622.
- [21] P. Jenny, S. H. Lee, and H. A. Tchelepi, Adaptive fully implicit multi-scale finite-volume method for multi-phase flow and transport in heterogeneous porous media, J. Comput. Phys. 217(2) (2006), 627–641.
- [22] A. M. JONES, P. A. BOSLER, P. A. KUBERRY, AND G. B. WRIGHT, Generalized moving least squares vs. radial basis function finite difference methods for approximating surface derivatives, Comput. Math. Appl. 147 (2023), 1–13.
- [23] Q. LI AND L. MEI, Efficient, decoupled, and second-order unconditionally energy stable numerical schemes for the coupled Cahn-Hilliard system in copolymer/homopolymer mixtures, Comput. Phys. Commun. 260 (2021), 107290.
- [24] T. LI, P. LIU, J. ZHANG, AND X. YANG, Efficient fully decoupled and second-order time-accurate scheme for the Navier-Stokes coupled Cahn-Hilliard Ohta-Kawaski phase-field model of diblock copolymer melt, J. Comput. Appl. Math. 403 (2022), 113843.
- [25] H. Manzanarez, J. P. Merico, P. Guenoun, J. Chikina, and D. Bouyer, *Modeling phase inversion using Cahn-Hilliard equations-Influence of the mobility on the pattern formation dynamics*, Chem. Eng. Sci. 173 (2017), 411–427.
- [26] V. Mohammadi and M. Dehghan, Simulation of the phase field Cahn-Hilliard and tumor growth models via a numerical scheme: Element-free Galerkin method, Comput. Methods Appl. Mech. Eng. 345 (2019), 919–950.
- [27] D. O'CONNOR, Phase field models on evolving surfaces, University of Warwick, 2016.
- [28] J. H. Park, A. J. Salgado, and S. M. Wise, Benchmark computations of the phase field crystal and functionalized Cahn-Hilliard equations via fully implicit. Nesterov accelerated schemes, arXiv:2204.07247, 2022.

- [29] A. Petras, L. Ling, C. Piret, and S. J. Ruuth, A least-squares implicit RBF-FD closest point method and applications to PDEs on moving surfaces, J. Comput. Phys. 381 (2019), 146–161.
- [30] R. Ruiz, R. L Sandstrom, and C. T. Black, *Induced orientational order in symmetric diblock copolymer thin films*, Adv. Mater. 19(4) (2007), 587–591.
- [31] S. Samimi and A. Pak, A novel three-dimensional element free Galerkin (EFG) code for simulating two-phase fluid flow in porous materials, Eng. Anal. Bound. Elem. 39 (2014), 53–63.
- [32] J. Shen, Long time stability and convergence for fully discrete nonlinear Galerkin methods, Appl. Anal. 38(4) (1990), 201–229.
- [33] J. Shen and X. Yang, *Numerical approximations of Allen-Cahn and Cahn-Hilliard equations*, Discrete Contin. Dyn. Syst 28(4) (2010), 1669–1691.
- [34] X. F. WU AND Y. A. DZENIS, Phase-field modeling of the formation of lamellar nanostructures in diblock copolymer thin films under inplanar electric fields, Phys. Rev. E 77(3) (2008), 031807.
- [35] X. XIAO, X. FENG, AND Z. SHI, Efficient numerical simulation of Cahn-Hilliard type models by a dimension splitting method, Comput. Math. Appl. 136 (2023), 54–70.
- [36] C. Xu and T. Tang, Stability analysis of large time-stepping methods for epitaxial growth models, SIAM J. Numer. Anal. 44(4) (2006), 1759–1779.
- [37] J. Zhang, C. Chen, and X. Yang, *Efficient and energy stable method for the Cahn-Hilliard phase-field model for diblock copolymers*, Appl. Numer. Math. 151 (2020), 263–281.